Journal of Cancer Research and Clinical Oncology (2019) 145:2937–2950
https://doi.org/10.1007/s00432-019-03048-1

ORIGINAL ARTICLE – CANCER RESEARCH

Are shape morphologies associated with survival? A potential shape-based biomarker predicting survival in lung cancer

Maliazurina Saad[1] · **Ik Hyun Lee**[2] · **Tae-Sun Choi**[3]

Received: 25 February 2019 / Accepted: 4 October 2019 / Published online: 16 October 2019

Abstract

Purpose Imaging biomarkers (IBMs) are increasingly investigated as prognostic indicators. IBMs might be capable of assisting treatment selection by providing useful insights into tumor-specific factors in a non-invasive manner.

Methods We investigated six three-dimensional shape-based IBMs: eccentricities between (I) intermediate–major axis (E_{imaj}), (II) intermediate–minor axis (E_{imin}), (III) major–minor axis ($E_{mj\text{-}mn}$) and volumetric index of (I) sphericity (*VioS*), (II) flattening (*VioF*), (III) elongating (*VioE*). Additionally, we investigated previously established two-dimensional shape IBMs: eccentricity *(E)*, index of sphericity *(IoS)*, and minor-to-major axis length *(Mn_Mj)*. IBMs were compared in terms of their predictive performance for 5-year overall survival in two independent cohorts of patients with lung cancer. Cohort 1 received surgical excision, while cohort 2 received radiation therapy alone or chemo-radiation therapy. Univariate and multivariate survival analyses were performed. Correlations with clinical parameters were evaluated using analysis of variance. IBM reproducibility was assessed using concordance correlation coefficients (CCCs).

Results *E* was associated with reduced survival in cohort 1 (hazard ratio [HR]: 0.664). E_{imin} and *VioF* were associated with reduced survival in cohort 2 (HR 1.477 and 1.701). *VioS* was associated with reduced survival in cohorts 1 and 2 (HR 1.758 and 1.472). Spherical tumors correlated with shorter survival durations than did irregular tumors (median survival difference: 1.21 and 0.35 years in cohorts 1 and 2, respectively). *VioS* was a significant predictor of survival in multivariate analyses of both cohorts. All IBMs showed good reproducibility (CCC ranged between 0.86–0.98).

Conclusions In both investigated cohorts, *VioS* successfully linked shape morphology to patient survival.

Keywords Imaging biomarker · Tumor shape · Non-small cell lung cancer · Prognosis · Overall survival

Introduction

Lung cancer has been one of the leading causes of death in South Korea and has been the country's major public health concern since 1983. In 2018, an estimated 26,725 of new lung cancer cases occurred with 19,317 deaths (Jung et al. 2018). Prognostic algorithms in palliative and curative settings include an integrated evaluation of clinico-pathologic, histo-morphologic, and radio-morphologic findings (Cohen et al. 2016; Lederlin et al. 2013). The combination of these parameters often reveals the prognostic effect of postoperative treatment (Hattori et al. 2017; Raghunath et al. 2014). Despite therapeutic advances in lung cancer, the overall survival rate remains disappointingly low (Siegel et al. 2017; Jung et al. 2016). The major impediment to successful treatment is the fact that histologically similar tumors display a wide range of treatment responses and metastatic behaviors (Kratz et al. 2012; Saad and Choi 2017, 2018). The identification of oncogenic drivers and tumor suppressor genes (Oxnard et al. 2013; El-Telbany and Ma 2012) has shed some light on molecular targeted therapy; however, recent studies in the field of biomedical informatics have begun to link imaging features to gene expression, giving rise to the fields of radiomics and radio-genomics (Wang et al. 2016;

Electronic supplementary material The online version of this article (https://doi.org/10.1007/s00432-019-03048-1) contains supplementary material, which is available to authorized users.

✉ Maliazurina Saad
mbs@illinois.edu

[1] University of Illinois at Urbana-Champaign, 1406 W Green St, Urbana, IL 61801, USA

[2] Korea Polytechnic University, Siheung, Korea

[3] Gwangju Institute of Science and Technology, Gwangju, Korea

Aerts et al. 2014; Ellingson 2015). These developments have supported the idea that molecular-level activities may be reflected in imaging phenomena.

It has been hypothesized that imaging features could be used as independent prognostic biomarkers for additional insight, as a means of supplementing clinical and molecular information during clinical decision making (Gevaert et al. 2012). These patient-specific biomarkers have the potential to individualize and improve patient outcomes. Several studies have investigated the association between shape-based imaging biomarkers (IBMs) and the prognosis of patient outcomes in non-small cell lung cancer (NSCLC). Baba et al. (2012) introduced the ratio of minor to major axis length that separated tumors into globular and ellipsoidal groups. Koo et al. (2017) proposed areas that predict recurrence in surgically resected tumors. Grove et al. (2015) proposed that convexity was associated with overall survival. In another work, tumor volume (Bianconi et al. 2018; Huynh et al. 2016) and F2 (Li et al. 2017) also demonstrated a good prognostic value. Nonetheless, there have been several studies with negative findings such as those shown in (Sacconi et al. 2017; Song et al. 2016), where none of the shape features tested correlated with any clinical outcomes. However, these studies mostly focused on a two-dimensional (2D) plane; whereas the work that can be considered as a three-dimensional (3D) approach used conventional feature like volume. On top of that little to no information regarding the reliability of the proposed IBMs was presented.

In this study, we aimed to investigate the possibility of correlations between shape morphologies and patient survival by evaluating nine shape-based features. Of these nine features, six are newly introduced as modifications of previously proposed 2D versions (Baba et al. 2012; Ionescu-Tirgoviste et al. 2015; Thomas Jr and Finney 1979). We tested the hypothesis that the modified 3D versions provide better representations of tumor shape morphology, as compared with the 2D versions, which focus on the largest tumor diameter. A better morphological representation may have a better correlation with survival.

Materials and methods

Patient population

The imaging data of patients diagnosed with primary NSCLC were collected from a public repository, the cancer imaging archive (TCIA) (Clark et al. 2013) and curated into two independent cohorts. Cohort 1 consisted of patients who received surgical resection; the data from this cohort include CT and PET/CT images, segmentation maps of the tumor, RNA sequencing data from surgically excised tumor tissue, and clinical data including survival outcomes. This cohort was originally assembled by Gevaert et al. (2012) as a 26-subject pilot dataset. Cohort 2 consisted of patients with unresectable tumors; their data include CT images of the tumor, manual delineation by a radiation oncologist of the 3D gross volume of the tumor, and clinical and outcome data. This cohort was assembled from the TCIA following the methods of Aerts et al. (2014) and included the same patients. Regarding inclusion criteria, cohort 1 included patients of all disease stages, whereas cohort 2 only included patients who have no metastases. In both cohorts, subjects with incomplete medical records were excluded. Cohorts 1 and 2 were from different medical centers. Cohort 1 consisted of 74.5% male subjects with a mean age of 71.8 years; cohort 2 consisted of 71.5% male subjects with a mean age of 66.7 years. CT examinations were acquired using CT scanners manufactured by CMS, Siemens, and GE Medical Systems.

The duration of overall survival (OS) was calculated from the date of the first treatment received to the last date at which the patient was known to be living. Survival distributions were summarized in terms of 5-year overall survival rates. Patient characteristics are summarized in Table 1.

The acquisition protocol varied slightly between cohorts. Exposure settings ranged 100–120 kVp in cohort 1 and 120–140 kVp in cohort 2. Pixel spacings ranged 0.5895–0.9765 mm in cohort 1 and 0.8120–0.9769 mm in cohort 2. Slice thicknesses ranged 0.60–3.75 mm in cohort 1, but were the same for all patients in cohort 2 (3.0 mm). All images were reconstructed as 512×512 pixel matrices.

Tumor delineation

Both cohorts were supplied with pre-defined lesion locations, but manual extraction work was still required. The extraction of these region of interests (ROIs) was facilitated by an automated extraction tool developed based on geometrical and topological processing (Saad et al. 2019). This tool eliminated the manual delineation work that was required in this study.

IBM design

Physicians often semantically describe lung tumor morphology using radiologic lexicons such as lobulated or spiculated (tumor margin), spherical or irregular (tumor shape), solid or opacity (tissue attenuation), and cavitation, cyst, or reticulation (internal characteristic). However, these lexicons are subjective; thus, the quantification of these terminologies using computer usable forms is favored. To reduce complexity, this study only focused on the shape-based terminology: spherical vs irregular tumors. Three 2D features were selected as the foundation (Online Resource 1). Based on these features, six 3D features quantifying the shape morphology were

Table 1 Demographics, disease staging, histological types, imaging protocols, and clinical outcomes for both tested cohorts

Characteristics	Cohort 1		Cohort 2	
	Total (/145)	(%)	Total (/123)	(%)
Sex				
Male	108	74.5	88	71.5
Female	37	25.5	35	28.5
Age (years)				
≤ 70	84	57.9	68	55.3
> 70	61	42.1	55	44.7
Pathological staging				
Primary tumor T				
I	74	51.0	27	22.0
II	49	33.8	46	37.4
III	17	11.7	14	11.4
IV	5	3.4	36	29.3
Lymph node N				
0	117	80.7	53	43.1
1	12	8.3	7	5.7
2	16	11.0	37	30.1
3	0	0.0	26	21.1
Metastasis M				
0	142	97.9	123	100.0
1	3	2.1	0	0.0
Histology				
Squamous cell	30	20.7	39	31.7
Non-squamous cell	115	79.3	84	68.3
5-year survival				
Survived	52	35.9	4	3.3
Expired	93	64.1	119	96.7
Imaging protocols				
Pixel spacing (mm)				
≤ 0.90	128	88.3	2	1.6
> 0.90	17	11.7	121	98.4
Slice thickness (mm)				
< 3.0	139	95.9	0	0.0
≥ 3.0	6	4.1	123	100.0
Convolution kernel				
LUNG	64	44.1	0	0.0
STANDARD	30	20.7	0	0.0
B30f	0	0.0	33	26.8
B31f	1	0.7	14	11.4
Others	50	34.5	76	61.8

introduced. Figure 1 presents how we modified eccentricity (*E*) and minor to major axis length (*Mn_Mj*) approaches in quantifying the eccentricity from a 3D perspective using three semi-axes length (*a*, *b*, and *c*) or also known as principal moments of inertia. The first two equations give eccentricity measured between semi-intermediate axis *b* and semi-major axis *a* or semi-minor axis *c*. Equation 3 quantifies the difference in eccentricity between those two perpendicular planes as previously measured in Eq. (1–2). Measurements ranged between 0–1, with 0 indicating an object that is a perfect sphere.

$$E_{imaj} = \sqrt{a^2 - b^2} \tag{1}$$

$$E_{imin} = \sqrt{b^2 - c^2} \tag{2}$$

$$E_{mj-mn} = \sqrt{\left(E_{imaj} - E_{imin}\right)^2} \tag{3}$$

Figure 2 demonstrates the fundamental aspects underlying the introduction of Eqs. (4–6), which describes the shape complexity of an object by determining the actual and ideal shapes. This technique was first introduced by Ionescu-Tirgoviste et al. (2015) and is called index of sphericity, which measures the circularity of 2D objects. We proposed a similar approach on 3D planes via the principle of ellipsoid of revolution. Three ideal shapes were defined in this study: (i) sphere (a = b = c), (ii) sphere that is flattened along the horizontal plane (a = b > c), and (iii) sphere that is elongated along the vertical plane (a = b < c). First, the surface area to volume ratio was calculated for each ideal case; for example, the sphere case was given by $(4\pi r^2 / \frac{4}{3}\pi r^3)$.

Second, an assumption was made that the tumors were not in ideal forms, having distinct lengths for all semi-axes (a ≠ b ≠ c) and, thus, *r* in the surface area to volume ratio was replaced by the average of the three semi- axes. Following these derivations, *VioS* as depicted by Eq. (4) measures a tumor's divergence from a perfect sphere. The fifth proposed marker *VioF* as shown in Eq. (5) refers to the measurement of a tumor that is elongated along the horizontal plane, whereas *VioE* as depicted by Eq. (6) quantifies the amount of compression that happens on the vertical plane, specifically for those tumors that exhibit an egg shape. *VioF* and *VioE* are meant for tumors located around the pleural and mediastinum window that may have a growth pattern that is stretched vertically or horizontally, resulting from the tumor pressing against the pleural or mediastinal wall. The closer a measurement is to 1, the closer the pattern is to the ideal shape, which indicates that the difference of that particular pattern to the ideal shape is small.

$$VioS = \frac{I_{AS}}{I_{IS}}, \tag{4}$$

$$VioF = \frac{I_{AS}}{I_{OS}}, \tag{5}$$

$$VioE = \frac{I_{AS}}{I_{PS}}. \tag{6}$$

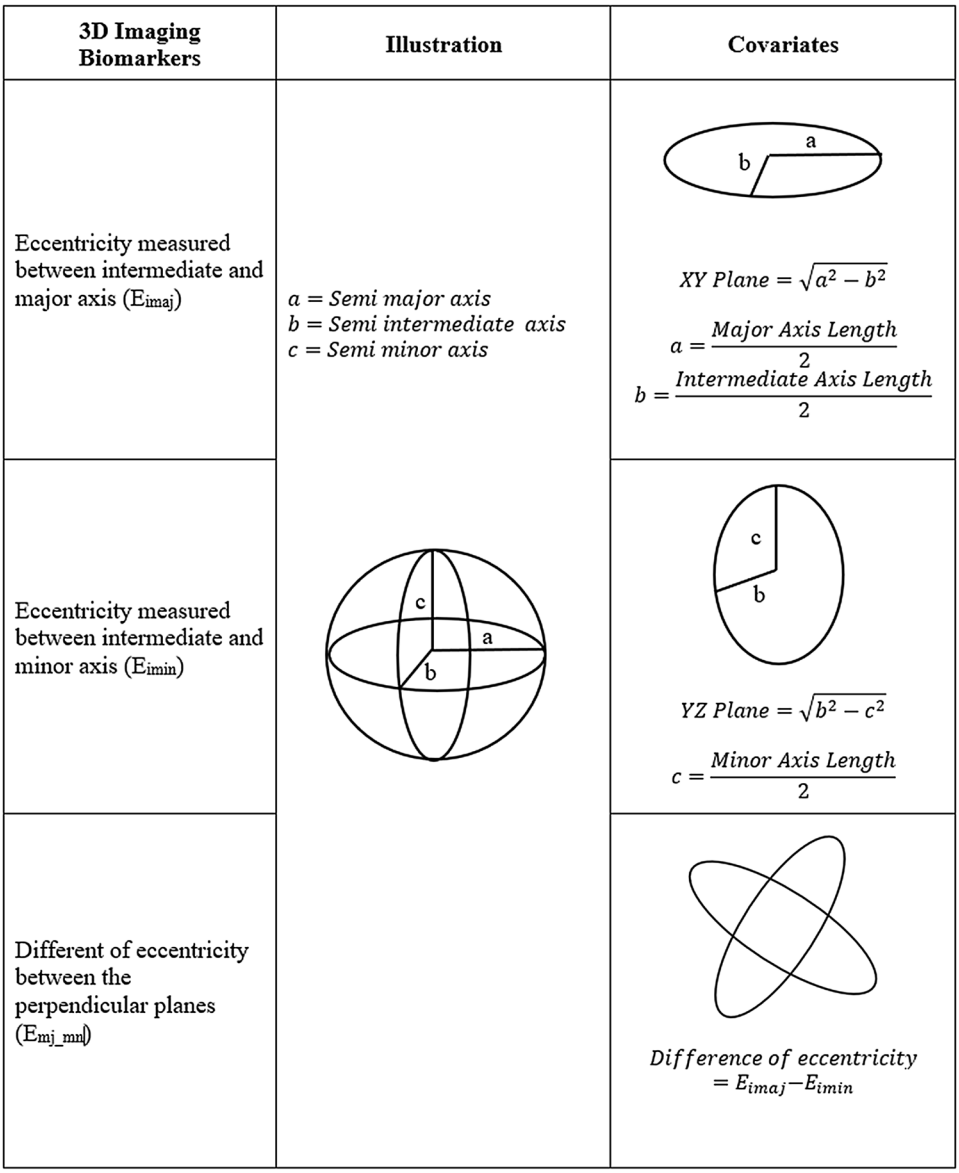

Fig. 1 Three dimensional eccentricity; E_{imaj}, E_{imin}, and $E_{mj\text{-}mn}$ were constructed based on 2D version of eccentricity using principle axes theorem

Association with 5-year survival and the prognostic impact

The following uni- and multivariable methods were used in the survival analysis: Kaplan–Meier (KM) curve, log-rank test (p value), and Cox proportional hazards model. KM estimator was used to estimate the survival function from life-time data; for example, the fraction of patients living for a certain length of time after treatment (Goel et al. 2010), while the log-rank test was used to compare survival curves obtained by KM analysis. Both KM and log-rank test are examples of univariable analysis and non-parametric statistics. They describe survival according to one factor under investigation, but ignore the impact of others. On the other hand, Cox proportional hazards modeling is a regression model used to adjust survival for potential confounders. It allows the examination on how specific covariates influence the event of interest at a point of time. The rate is known as hazard ratio (Christensen 1987). Statistical significance is given by two-tailed p values lower than 0.05. The subjects were divided into two comparative groups: spherical or irregular tumor using the proposed IBMs through an unsupervised learning algorithm, fuzzy C-means clustering (Chattopadhyay et al. 2012). Instead of following the traditional method of dividing the subjects by manually setting a threshold, we let the artificial intelligence program determine the division. Fuzzy C-means clustering (FCM) involves assigning elements to clusters $\{C_j\}_{j=1}^{m}$ such that elements in the same cluster are as similar as possible, while elements belonging to different cluster are as dissimilar as possible. The

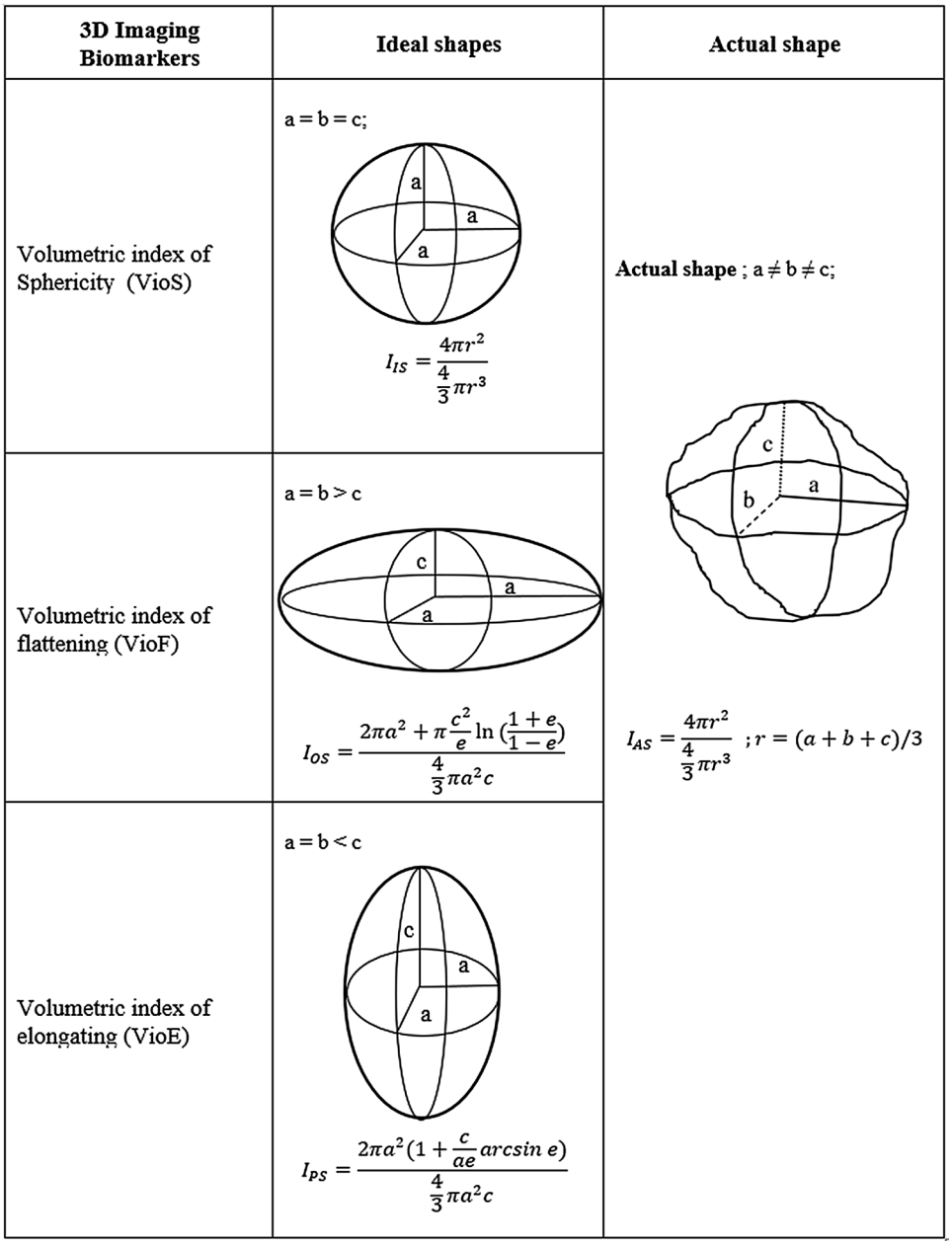

Fig. 2 Three dimensional measurements of shape complexity; *VioS*, *VioF*, and *VioE* were constructed based on the principle of ellipsoid of revolution

clusters are identified via similarity measures. E.g., given a set of elements$\{x_1, x_2, \ldots. x_n\}$, FCM returns a list of cluster centers $\{C_1, \ldots. C_m\}$ and a membership matrix $U = U_{ij} \in [0,1]$, $i = 1 \ldots n$, $j = 1 \ldots m$, where each element U_{ij} represents the degree to which element x_i belongs to cluster C_j. In our case, the FCM algorithm attempts to partition a group of n tumors into m clusters ($m = 2$) with respect to their shape complexity. The algorithm is based on minimization of an objective function as represented by Eq. (7).

$$J_m = \sum_{i}^{N}\sum_{j}^{C} u_{ij}^{m}\left\|x_i - c_j^2\right\|. \tag{7}$$

In Eq. (7), m is the fuzziness exponent, N is the number of instances, C is the number of cluster, u_{ij} is the membership matrix, x_i is data in ith element, and c_j is the cluster number.

The prognostic impact of each IBM was associated with demographics (age and sex), pathological staging (primary tumor T, lymph node invasion N, and metastasis M), gene profile (*EGFR*, *KRAS*, and *ALK*), and the imaging parameters (slice thickness, pixel spacing, and convolution kernel) in cohort 1; in cohort 2, the gene profile correlation was omitted because the required information was not provided.

Reproducibility analysis

Reproducibility is an important trait for biomarker development. An independent cohort of 32 subjects, with same-day repeat CT scans, was used as our test–retest environment (Zhao et al. 2009). The baseline and follow-up scans were obtained within an interval of 15 min of each other, using an identical CT scanner and imaging protocols. The concordance correlation coefficient (CCC), a metric that quantifies the degree of agreement between two pairs of observations, was used. The CCC evaluates the degree of agreement with which a pair of observations falls on the 45° line through the origin (Lawrence and Lin 1989). All algorithms were implemented using MATLAB (R2015b; MathWorks, Inc., Natick, MA, USA) and all statistical analyses were conducted using MedCalc Statistical Software (version 18.11; Ostend, Belgium).

Results

Establishing the correlation of shape morphologies to the 5-year OS

Table 2 presents the univariable analyses conducted in cohort 1 and cohort 2. In cohort 1, the parameters *E* (HR 0.664, [0.430–1.025]) and *VioS* (HR 1.760, [1.171–2.644]) from 2D and 3D IBM, respectively, showed statistically

Table 2 Univariable survival analyses for the two-dimensional and three-dimensional imaging biomarkers in cohorts 1 and 2

Biomarkers	Cohort 1			Cohort 2		
	HR	95% CI	*p* value	HR	95% CI	*p* value
2-Dimensional						
E						
Spherical	1		**0.049***	1		0.160
Irregular	0.664	0.430–1.025		1.319	0.896–1.944	
Mn_Mj						
Spherical	1		0.052	1		0.504
Irregular	1.497	0.996–2.253		1.137	0.779–1.660	
IoS						
Spherical	1		0.122	1		0.203
Irregular	1.523	0.892–1.661		1.337	0.854–2.094	
3-Dimensional						
E_{imaj}						
Spherical	1		0.735	1		0.910
Irregular	0.929	0.606–1.424		0.978	0.665–1.437	
E_{imin}						
Spherical	1		0.131	1		**0.036***
Irregular	0.730	0.485–1.098		1.477	1.025–2.129	
$E_{mj\text{-}mn}$						
Spherical	1		0.086	1		0.119
Irregular	0.697	0.461–1.053		0.742	0.510–1.080	
VioS						
Spherical	1		**0.006***	1		**0.037***
Irregular	1.758	1.168–2.647		1.472	1.022–2.120	
VioF						
Spherical	1		0.166	1		**0.005***
Irregular	1.346	0.883–2.052		1.701	1.167–2.479	
VioE						
Spherical	1		0.109	1		0.098
Irregular	0.716	0.477–1.077		0.734	0.509–1.059	

HR hazard ratio, *CI* confidence interval, *E* eccentricity, *IoS* index of sphericity, *Mn_Mj* minor to major axis length, E_{imaj} eccentricity between intermediate-major axis, E_{imin} eccentricity between intermediate-minor axis, $E_{mj\text{-}mn}$ eccentricity difference on two perpendicular planes, *VioS* volumetric index of sphericity, *VioF* volumetric index of flattening, *VioE* volumetric index of elongation

Statistical significance ($p < 0.05$) is represented by the bold and *

Table 3 Mean survival as calculated from Kaplan-Meier survival curves. All values are presented in years

Biomarkers	Cohort 1			Cohort 2		
	Mean	95% CI	Difference	Mean	95% CI	Difference
2-Dimensional						
E						
Spherical	5.13	4.44–5.82	**0.97**	1.69	1.36–2.01	0.28
Irregular	4.16	3.23–5.09		1.97	1.62–2.32	
Mn_Mj						
Spherical	3.69	3.10–4.28	0.82	1.79	1.48–2.09	0.22
Irregular	4.51	3.83–5.20		2.01	1.59–2.44	
IoS						
Spherical	5.20	4.53–5.87	1.43	1.54	1.11–1.97	0.42
Irregular	3.77	2.65–4.90		1.96	1.67–2.26	
3-Dimensional						
E_{imaj}						
Spherical	5.02	4.27–5.77	0.39	1.85	1.53–2.17	0.04
Irregular	4.63	3.75–5.51		1.89	1.50–2.28	
E_{imin}						
Spherical	5.42	4.53–6.31	1.11	1.64	1.36–1.93	**0.54**
Irregular	4.31	3.62–5.06		2.18	1.75–2.62	
$E_{mj\text{-}mn}$						
Spherical	5.42	4.59–6.26	1.19	2.01	1.63–2.38	0.32
Irregular	4.23	3.47–4.99		1.69	1.37–2.00	
VioS						
Spherical	4.02	3.32–4.72	**1.81**	1.64	1.35–1.92	**0.53**
Irregular	5.83	4.94–6.71		2.17	1.74–2.60	
VioF						
Spherical	4.27	3.43–5.10	1.02	1.48	1.17–1.80	**0.75**
Irregular	5.29	4.52–6.07		2.23	1.88–2.59	
VioE						
Spherical	5.50	4.63–6.37	1.2	1.63	1.32–1.95	0.59
Irregular	4.30	3.56–5.04		2.22	1.85–2.60	

HR hazard ratio, *CI* confidence interval, *E* eccentricity, *IoS* index of sphericity, *Mn_Mj* minor to major axis length, E_{imaj} eccentricity between intermediate-major axis, E_{imin} eccentricity between intermediate-minor axis, $E_{mj\text{-}mn}$ eccentricity difference on two perpendicular planes, *VioS* volumetric index of sphericity, *VioF* volumetric index of flattening, *VioE* volumetric index of elongation

The bold values represent the mean survival difference of biomarkers with statistical significance as reported in Table 2

significant differences in survival between the two groups with irregular vs. spherical tumors. The multivariable analysis only retained *VioS* from the univariate pool as the sole and independent prognostic factor (HR 1.767 [1.162–2.686]). In cohort 2, none of the 2D IBMs reported statistically significant differences; however, three of the 3D IBMs demonstrated significant differences in survival between the two groups; E_{imin} (HR 1.469, [1.025–2.106]), *VioS* (HR 1.462, [1.020–2.094]), and *VioF* (HR 1.637, [1.131–2.369]). Of the variables that showed significant associations with survival in the univariate analyses, only *VioS* remained significantly prognostic in the multivariable analysis of cohort 2 (HR 1.665 [1.115–2.401]).

Following this observation, a comparison of overall survival time between the two groups was performed (Tables 3, 4). We observed that the mean survival differences between groups that were clustered using 2D IBMs ranged between 0.82–1.43 years and 0.22–0.42 years in cohort 1 and cohort 2, respectively (Table 3). The mean survival differences returned by 3D IBMs ranged between 0.39–1.81 years in cohort 1 and 0.04–0.75 years in cohort 2. The highlighted values in Table 3 represent the mean differences returned by those IBMs that showed statistical significance during univariable analysis as reported in Table 2.

Table 4 shows the median survival difference between the two groups. Differences in median survival reported by 2D IBMs ranged from 0.46–0.87 years to 0.01–0.33 years

Table 4 Median survival as calculated from Kaplan-Meier survival curves. All values are presented in years

Biomarkers	Cohort 1			Cohort 2		
	Median	95% CI	Difference	Median	95% CI	Difference
2-Dimensional						
E						
Spherical	3.96	3.48–5.04	**0.8**	1.49	1.14–193	0.01
Irregular	3.16	2.18–4.14		1.48	1.22–1.93	
Mn_Mj						
Spherical	3.21	2.49–4.14	0.87	1.74	1.25–2.48	0.33
Irregular	4.08	3.51–5.24		1.41	1.12–1.79	
IoS						
Spherical	3.50	1.45–4.42	0.46	1.39	0.71–1.79	0.19
Irregular	3.96	3.31–4.92		1.58	1.27–2.02	
3-Dimensional						
E_{imaj}						
Spherical	3.96	3.16–4.92	0.45	1.64	1.39–2.07	0.24
Irregular	3.51	2.96–4.35		1.40	1.04–1.75	
E_{imin}						
Spherical	4.08	3.48–4.92	0.57	1.41	0.85–1.79	**0.33**
Irregular	3.51	2.72–4.09		1.74	1.29–2.54	
$E_{mj\text{-}mn}$						
Spherical	4.24	3.48–4.99	0.82	1.44	1.21–1.93	0.05
Irregular	3.42	2.49–3.99		1.49	0.85–1.93	
VioS						
Spherical	3.21	2.49–3.84	**1.21**	1.39	0.85–1.79	**0.35**
Irregular	4.42	3.75–4.97		1.74	1.27–2.54	
VioF						
Spherical	3.48	2.47–4.24	0.60	2.09	1.41–2.78	**0.74**
Irregular	4.08	3.42–4.97		1.35	0.84–1.57	
VioE						
Spherical	4.14	3.42–4.97	0.64	2.31	1.44–2.92	0.96
Irregular	3.50	2.76–4.04		1.35	0.87–1.57	

HR hazard ratio, *CI* confidence interval, *E* eccentricity, *IoS* index of sphericity, *Mn_Mj* minor to major axis length, E_{imaj} eccentricity between intermediate-major axis, E_{imin} eccentricity between intermediate-minor axis, $E_{mj\text{-}mn}$ eccentricity difference on two perpendicular planes, *VioS* volumetric index of sphericity, *VioF* volumetric index of flattening, *VioE* volumetric index of elongation

The bold values represent the median survival difference of biomarkers with statistical significance as reported in Table 2

in cohort 1 and cohort 2, respectively; 3D IBMs ranged between 0.45–1.21 years in cohort 1 and 0.05–0.96 years in cohort 2. Therefore, four IBMs (*Mn_Mj, IoS, VioS, and VioF*), have shown consistency in predicting the group that has a better prognosis in both investigated cohorts wherein subjects with irregular shaped tumors have a longer survival time in comparison to the subjects with spherical tumors. The remaining IBMs were discarded as potential candidates due to the inconsistency shown between the two cohorts. Nonetheless, *VioS* was the only IBM from the final pool that is consistent in predicting the survival outcome with statistical significance during the univariable analysis (Table 2); based on these findings, we concluded that *VioS* could be a potential risk factor in predicting survival based on tumor shape. *VioS* revealed that spherical tumors have a worse prognosis, being 1.21 years lower in median survival for cohort 1 and 0.35 years lower in median survival for cohort 2, in comparison to the irregular tumors. The survival curves for *VioS* on both cohorts are provided as Online Resource 2. For visualization purposes on how *VioS* grouped the subjects according to their tumor shapes, we have included several examples from both cohorts in Figs. 3 and 4.

Clinico-radiological correlation to IBMs

These analyses were conducted to establish the correlation of the proposed IBMs to clinical factors as discussed in "Materials and methods" under *IBM Design*. The existing

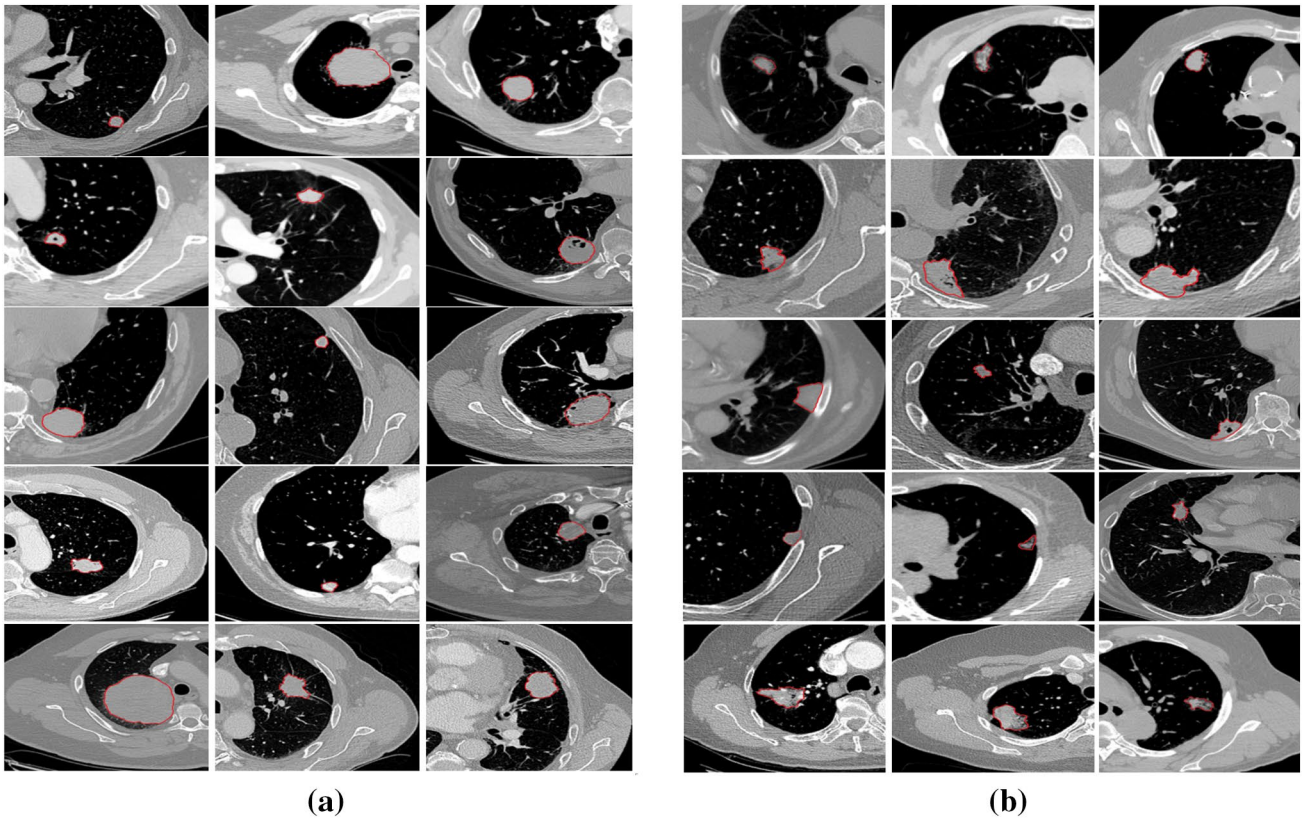

Fig. 3 Subjects in cohort 1 were clustered into **a** spherical and **b** irregular tumor shape according to their VioS values

2D IBMs were not investigated in this analysis. Tables 5 and 6 depict the statistical analyses performed through one-way analysis of variance (ANOVA), which measures the difference between the means of two subgroups. Demographically, *Age* and *Gender* were correlated to all IBMs, but only *VioE* showed statistical significance difference by *Age* ($p = 0.028$). Interestingly, all six IBMs demonstrated statistical significance in primary tumor *T*, but not in lymph node involvement *N* or metastasis *M* factor. Additionally, we did not observe a statistically significant difference for any of the three investigated gene mutation profiles (*EGFR, KRAS,* and *ALK*). The potential connection of imaging protocols to the IBMs was also investigated, in which mixed observations were noticed. Slice thickness was significant in *VioS*, *VioF,* and *VioE*, but not in any of the 3D eccentricities. Pixel spacing was only positively correlated to *VioE* and the convolution kernel showed no significance differences in any of the IBMs. We only included cohort 1 results in this section, while cohort 2 correlation results are presented in Online Resource 3.

Test–retest analysis

The reproducibility analysis was conducted on an independent cohort, separated from the two main cohorts to derive insights on the ability of the proposed image-based biomarkers to reproduce across different environments. We observed that three of the IBMs scored substantial amount of agreement between measurements taken on baseline versus follow-up scans; *VioS* (CCC: 0.906 (0.781–0.962)), *VioF* (CCC: 0.982 (0.955–0.992)), and *VioE* (CCC: 0.983 (0.959–0.993), but slightly lower for the other three, E_{imaj} (CCC: 0.868 (0.700–0.945)), E_{imin} (CCC: 0.899 (0.765–0.958)) and $E_{mj\text{-}mn}$ (CCC: 0.882 (0.727–0.951)). Measurements can greatly vary with changes in z or depth of the slices in this testing, because the proposed IBMs were measured in 3D planes. However, we believe that the lower agreement seen in eccentricity-based IBMs is because these IBMs were taken on 2D viewpoints in a 3D projection in comparison to the volumetric-based IBMs, which are considered true 3D projections. Despite this, the CCC ranges were acceptable.

Discussion

In this study, we have investigated the potential correlation of shape morphologies to survival in patients with lung cancer. Nine shape-based imaging biomarkers were tested for their value in predicting outcomes in two independent cohorts

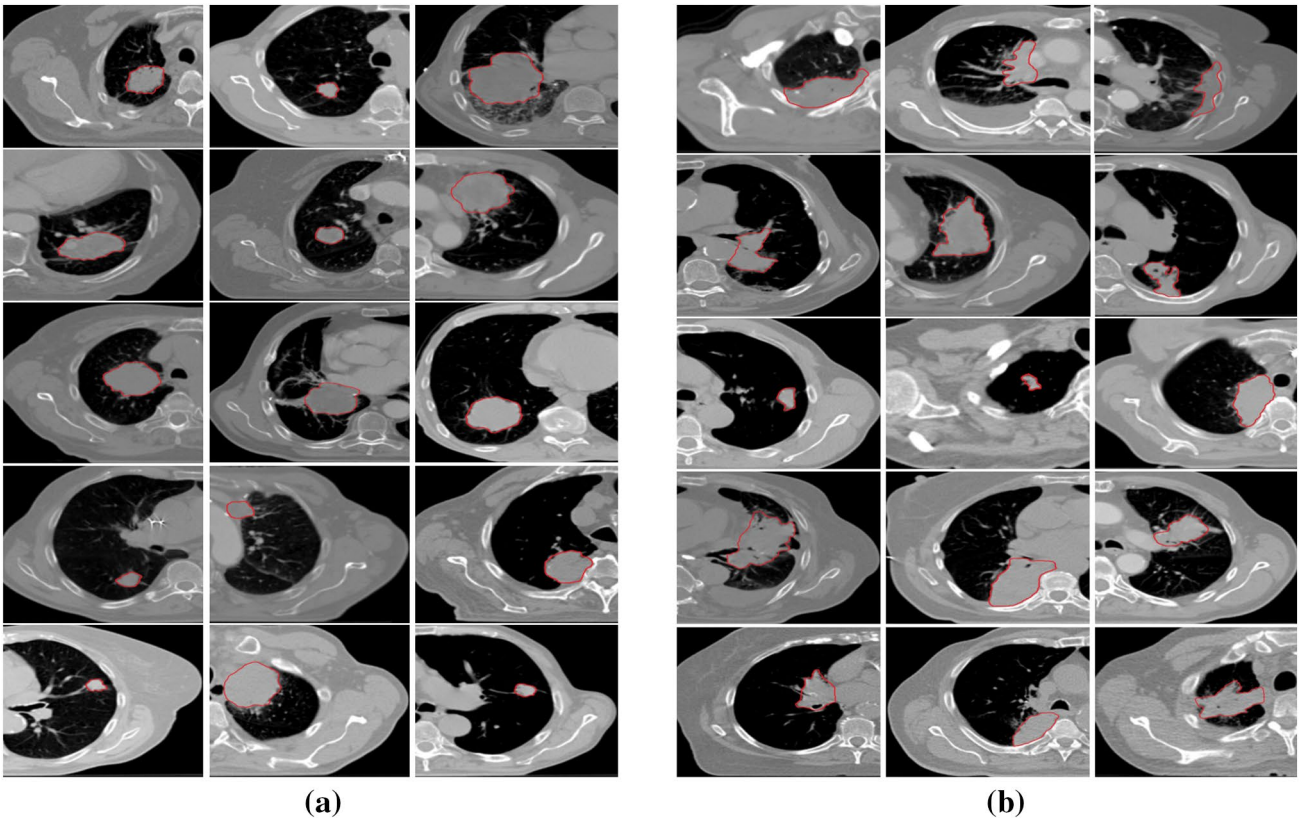

Fig. 4 Subjects in cohort 2 were clustered into **a** spherical and **b** irregular tumor shape according to their VioS values

of subjects with NSCLC; six of them (E_{imaj}, E_{imin}, $E_{mj\text{-}mn}$, *VioS*, *VioF* and *VioE*) were modified versions of the other three; *Mn-Mj* (Baba et al. 2012), *IoS* (Ionescu-Tirgoviste et al. 2015), and *E* (Thomas Jr and Finney 1979). We consistently found that irregular tumors had a better prognosis in both investigated cohorts predicted by four IBMs, including the ones introduced by Baba et al. (2012) and Ionescu-Tirgoviste et al. (2015). However, the univariable analyses only supported *VioS* as statistically significant in both cohorts. Following that observation, we concluded that *VioS* was a new potential risk factor predicting survival among NSCLC patients according to tumor shape morphology. The identification of imaging measures predicting NSCLC patient outcomes has been explored in several studies, including minor to major axis length predicting overall survival by Baba et al. (2012), tumor area and mean attenuation predicting recurrence by Koo et al. (2017), convexity and entropy ratio predicting overall survival by Grove et al. (2015); however, to the best of our knowledge, this is the first study that made comparisons between the prognostic impact provided by 2D and 3D shape-based imaging measures.

The key differences of this work are outlines as follows: firstly, we have modified the 2D quantifications of grouping tumor morphologies into spherical and non-spherical into a modified version from 3D projections. Instead of focusing on the CT slice with the largest tumor diameter (2D), the measurements considered the tumor as a whole (volumetric). The findings support the hypothesis that measuring tumors as a volume better predicts patient survival. Secondly, to provide insights into how shape morphology obtained by either 2D or 3D is associated with outcome, we compared the two versions; again, the null hypothesis was rejected. Thirdly, our investigation involved larger cohorts from two different centers in comparison to the previous work. This approach is believed to increase external validity, because generalization of conclusions derived from larger cohorts selected from multiple centers is more reliable. Lastly, instead of manually dividing the subjects by setting a threshold value, FCM was used to automate the intended work. It is, however, advisable to run the algorithms multiple times before drawing inference about the clusters. Being a non-deterministic approach by nature, one could possibly get unidentical results on multiple runs. One of the possible solutions to this issue would be to use a majority vote to determine the class that a data belongs to after several runs. On top of that, it is also possible to set a similar seed value on each run, thus eliminating the randomness which will lead to a deterministic result.

The survival outcomes inferred that patients with spherical tumors have worse lung cancer survival than patients with irregular or non-spherical tumors, which is congruent

Table 5 The correlation of E_{imaj}, E_{imin}, and $E_{mj\text{-}mn}$ with the clinical and imaging covariates in cohort 1

Biomarkers	E_{imaj}			E_{imin}			$E_{mj\text{-}mn}$		
	Mean	SD	*p* value	Mean	SD	*p* value	Mean	SD	*p* value
Demographics									
Age (years)									
≤70/83	0.60	0.16	0.716	0.75	0.11	0.687	0.24	0.19	0.615
>70/62	0.59	0.18		0.76	0.12		0.26	0.23	
Sex									
Male/108	0.60	0.16	0.929	0.76	0.13	0.923	0.26	0.22	0.565
Female/37	0.59	0.17		0.75	0.11		0.24	0.21	
Pathological staging									
Primary tumor									
T1/74	0.61	0.16	**0.005***	0.75	0.12	**0.004***	0.23	0.20	**0.028***
T2/49	0.63	0.13		0.74	0.11		0.21	0.16	
T3/17	0.49	0.20		0.83	0.09		0.35	0.28	
T4/5	0.45	0.26		0.87	0.16		0.42	0.42	
Lymph node									
N0/117	0.60	0.17	0.833	0.75	0.12	0.470	0.24	0.21	0.923
N1/12	0.59	0.15		0.76	0.13		0.27	0.16	
N3/16	0.57	0.18		0.79	0.12		0.24	0.28	
Metastasis									
M0/142	0.60	0.17	0.888	0.75	0.12	0.738	0.25	0.21	0.665
M1/3	0.58	0.07		0.78	0.01		0.19	0.09	
Gene mutations									
EGFR									
Wildtype/94	0.60	0.16	0.935	0.75	0.12	0.749	0.25	0.20	0.945
Mutant/23	0.59	0.17		0.77	0.10		0.24	0.21	
Unknown/28	0.59	0.20		0.74	0.13		0.26	0.25	
KRAS									
Wildtype /88	0.59	0.16	0.417	0.77	0.12	0.380	0.25	0.21	0.445
Mutant/27	0.64	0.13		0.73	0.11		0.20	0.16	
Unknown/30	0.59	0.20		0.75	0.13		0.26	0.24	
ALK									
Wildtype /109	0.59	0.16	0.897	0.76	0.12	0.831	0.25	0.21	0.661
Translocated/2	0.65	0.09		0.74	0.07		0.11	0.12	
Unknown/34	0.60	0.19		0.75	0.12		0.25	0.23	
Imaging protocol									
Slice thickness (mm)									
≤ 1.5/119	0.59	0.17	0.692	0.75	0.12	0.816	0.25	0.22	0.845
> 1.5/26	0.61	0.14		0.76	0.11		0.24	0.15	
Pixel spacing (mm)									
≤ 0.75/48	0.59	0.14	0.873	0.77	0.11	0.409	0.25	0.16	0.807
> 0.75/97	0.60	0.18		0.75	0.12		0.24	0.23	
Convolution kernel									
STANDARD/30	0.56	0.13	0.393	0.79	0.09	0.112	0.25	0.18	0.742
LUNG/64	0.61	0.18		0.73	0.12		0.23	0.22	
Others/51	0.59	0.18		0.76	0.13		0.26	0.22	

E_{imaj} eccentricity between intermediate-major axis, E_{imin} eccentricity between intermediate-minor axis, $E_{mj\text{-}mn}$ eccentricity difference on two perpendicular planes, *SD* standard deviation

Statistical significance ($p < 0.05$) is represented by the bold and *

Table 6 The correlation of *VioS, VioF*, and *VioE* with the clinical and imaging covariates in cohort 1

Biomarkers	*VioS*			*VioF*			*VioE*		
	Mean	SD	*p* value	Mean	SD	*p* value	Mean	SD	*p* value
Demographics									
Age (years)									
≤70/83	1.05	0.11	0.248	0.86	0.18	0.06	1.21	0.41	**0.028***
>70/62	1.07	0.12		0.80	0.18		1.06	0.39	
Sex									
Male/108	1.06	0.12	0.582	0.82	0.19	0.554	1.14	0.41	0.630
Female/37	1.05	0.11		0.85	0.16		1.18	0.40	
Pathological staging									
Primary tumor									
T1/74	1.04	0.10	**0.003***	0.87	0.17	**0.014**	1.25	0.40	**0.008***
T2/49	1.06	0.11		0.79	0.18		1.05	0.39	
T3/17	1.16	0.12		0.74	0.20		0.95	0.39	
T4/5	1.09	0.18		0.89	0.14		1.26	0.35	
Lymph node									
N0/117	1.05	0.11	0.303	0.84	0.18	0.282	1.18	0.40	0.226
N1/12	1.09	0.13		0.77	0.19		1.00	0.38	
N2/16	1.10	0.12		0.79	0.21		1.06	0.42	
Metastasis									
M0/142	1.06	0.12	0.896	0.83	0.18	0.988	1.15	0.40	0.989
M1/3	1.05	0.10		0.84	0.21		1.15	0.51	
Gene mutations									
EGFR									
Wildtype/94	1.06	0.12	0.491	0.82	0.20	0.188	1.13	0.43	0.210
Mutant/23	1.08	0.10		0.83	0.13		1.08	0.31	
Unknown/28	1.04	0.11		0.89	0.15		1.27	0.36	
KRAS									
Wildtype/88	1.07	0.11	0.770	0.83	0.16	0.282	1.14	0.38	0.511
Mutant/27	1.06	0.13		0.79	0.24		1.10	0.49	
Unknown/30	1.05	0.12		0.87	0.18		1.22	0.39	
ALK									
Wildtype /109	1.07	0.12	0.509	0.82	0.19	0.160	1.13	0.41	0.227
Translocated/2	1.11	0.01		0.68	0.26		0.84	0.42	
Unknown/34	1.04	0.11		0.88	0.16		1.23	0.37	
Imaging protocol									
Slice thickness (mm)									
≤ 1.5/119	1.05	0.12	**0.026***	0.86	0.18	**<0.001***	1.21	0.40	**<0.001***
> 1.5/26	1.11	0.10		0.71	0.15		0.87	0.28	
Pixel spacing (mm)									
≤ 0.75/48	1.08	0.10	0.203	0.79	0.16	0.059	1.04	0.37	**0.021***
> 0.75/97	1.05	0.12		0.85	0.19		1.20	0.41	
Convolution kernel									
STANDARD/30	1.09	0.11	0.158	0.82	0.19	0.235	1.16	0.46	0.122
LUNG/64	1.04	0.12		0.86	0.18		1.22	0.41	
Others/51	1.08	0.11		0.80	0.17		1.06	0.36	

VioS volumetric index of sphericity, *VioF* volumetric index of flattening, *VioE* volumetric index of elongation, *SD* standard deviation

Statistical significance ($p < 0.05$) is represented by the bold and *

with the findings in previous studies (Lederlin et al. 2013; Baba et al. 2012). However, contradicted finding was demonstrated in (Sacconi et al. 2017; Song et al. 2016). In their work, sphericity was not a prognostic predictor to survival. One possible root cause to this contradicted finding observed could be given by the fact that Sacconi et al., and Song et al., both used proprietary and conventional CT features in comparison to our work. There was no feature engineering work reported. It is assumed that irregular tumors have formed due to limitations in nutrient supply through vessels such as the bronchus and the lymphatic tissue, or inhibition by the lung immune system, whereas spherical tumors are formed through the uninhibited expanding and invasive nature of cancer cells. Our finding could be used to improve survival of patients with NSCLC by providing additional therapeutic interventions to patients with higher risk. The proposed markers may provide alternative factors for oncologists investigating tumor-specific factors during treatment planning: they are collected through less invasive methods than biopsy or resection sampling. The concept of using imaging measures as biomarkers is not new (Saad and Choi 2017, 2018; Aerts et al. 2014; Ellingson 2015), but the thought of having to go through complex imaging analysis with advance software may have hindered the unique benefit it can provide. Imaging biomarkers are the corner stone of modern radiology and may become major contributors to therapeutic decisions and drug evaluation in the near future. Therefore, multidisciplinary expertise is needed to facilitate this progress. It is worth mentioning that during our study, we noticed that some of the tumors were cavitated. It is possible that scoring the tumors based on the extent of cavitation, e.g., score = 1 (less than 50% cavitation) and score = 2 (more than 50% cavitation) could be another potential tumor-specific factor of prognostic value for NSCLC patients.

This study is, however, not without limitations. One general limitation of the study is the design, which was based on previous collected data and their retrospective analysis. Therefore, further prospective studies are warranted. Because the enrollment criteria were not restricted to a certain cancer stage, the conclusions were derived from data that include all stages of NSCLC. Therefore, it is inconclusive if the generalization of the proposed shape-based biomarkers to all cancer stages is possible. We also had to exclude a rather large number of subjects with incomplete clinical records from both cohorts and currently the study conclusions were derived from only one tumor site which is in the lung. It would be interesting if we could compare the prognostic indicator *VioS* in different cancer sites such as oral cancer as the same findings were documented in (Tarsitano et al. 2019) that the sphericity of a tumor was closely associated with death and recurrence. This could be a good validation in future study following this work. Despite these limitations, we are confident that as more data become available, the current model can be improved and can lead to more discoveries to enhance cancer care.

Acknowledgements This study was funded by the National Research Foundation of Korea (NRF) grants funded by the Korea government (MSIP) (Grant numbers NRF-2015R1A2A1A15053854 and NRF-2015R1A2A2A01002734).

Data availability The datasets analyzed during the current study are available from the cancer imaging archive (TCIA) repository (www.cancerimagingarchive.net).

Compliance with ethical standards

Conflict of interest The authors declare that they have no conflict of interest.

Ethical approval This study used data from a publicly available archive, the cancer imaging archive (www.cancerimagingarchive.net); hence, neither informed consent nor ethics approval prior to the study was necessary. However, the original authors who submitted the datasets to TCIA mentioned that the datasets are IRB approved. These collections are freely available to browse, download, and use for commercial, scientific, and educational purposes as outlined in the Creative Commons Attribution 3.0 Unported License.

References

Aerts HJ, Velazquez ER, Leijenaar RT et al (2014) Decoding tumour phenotype by noninvasive imaging using a quantitative radiomics approach. Nature Commun 5:4006

Baba T, Uramoto H, Takenaka M et al (2012) The tumour shape of lung adenocarcinoma is related to the postoperative prognosis. Interact Cardiovasc Thorac Surg 15:73–76

Bianconi F, Fravolini ML, Bello-Cerezo R et al (2018) Evaluation of shape and textural features from CT as prognostic biomarkers in non-small cell lung cancer. Anticancer Res 38:2155–2160

Chattopadhyay S, Pratihar DK, Sarkar SC (2012) A comparative study of fuzzy c-means algorithm and entropy-based fuzzy clustering algorithms. Comput Inform 30:701–720

Christensen E (1987) Multivariate survival analysis using Cox's regression model. Hepatology 7:1346–1358

Clark K, Vendt B, Smith K, Freymann J et al (2013) The cancer imaging archive (TCIA): maintaining and operating a public information repository. J Digit Imaging 26:1045–1057

Cohen JG, Reymond E, Jankowski A et al (2016) Lung adenocarcinomas: correlation of computed tomography and pathology findings. Diagn Interv Imaging 97:955–963

Ellingson BM (2015) Radiogenomics and imaging phenotypes in glioblastoma: novel observations and correlation with molecular characteristics. Curr Neurol Neurosci Rep 15:506

El-Telbany A, Ma PC (2012) Cancer genes in lung cancer: racial disparities: are there any? Genes Cancer 3:467–480

Gevaert O, Xu J, Hoang CD et al (2012) Non–small cell lung cancer: identifying prognostic imaging biomarkers by leveraging public gene expression microarray data—methods and preliminary results. Radiology 264:387–396

Goel MK, Khanna P, Kishore J (2010) Understanding survival analysis: Kaplan–Meier estimate. Int J Ayurveda Res 1:274

Grove O, Berglund AE, Schabath MB et al (2015) Quantitative computed tomographic descriptors associate tumor shape complexity and intratumor heterogeneity with prognosis in lung adenocarcinoma. PLoS One 10:e0118261

Hattori A, Matsunaga T, Hayashi T et al (2017) Prognostic impact of the findings on thin-section computed tomography in patients with subcentimeter non–small cell lung cancer. J Thorac Oncol 12:954–962

Huynh E, Coroller TP, Narayan V et al (2016) CT-based radiomic analysis of stereotactic body radiation therapy patients with lung cancer. Radiother Oncol 120:258–268

Ionescu-Tirgoviste C, Gagniuc PA, Gubceac E, Mardare L, Popescu I, Dima S, Militaru M (2015) A 3D map of the islet routes throughout the healthy human pancreas. Sci Rep 5:14634

Jung KW, Won YJ, Oh CM et al (2016) Prediction of cancer incidence and mortality in Korea, 2016. Cancer Res Treat 48:451–457

Jung KW, Won YJ, Kong HJ, Lee ES (2018) Prediction of cancer incidence and mortality in Korea, 2018. Cancer Res Treat 50:317–323

Koo HJ, Sung YS, Shim WH et al (2017) Quantitative computed tomography features for predicting tumor recurrence in patients with surgically resected adenocarcinoma of the lung. PLoS One 12:e0167955

Kratz JR, He J, Van Den Eeden SK et al (2012) A practical molecular assay to predict survival in resected non-squamous, non-small-cell lung cancer: development and international validation studies. Lancet 379:823–832

Lawrence I, Lin K (1989) A concordance correlation coefficient to evaluate reproducibility. Biometrics 45:255–268

Lederlin M, Puderbach M, Muley T et al (2013) Correlation of radio- and histomorphological pattern of pulmonary adenocarcinoma. Eur Respir J 41:943–951

Li Q, Kim J, Balagurunathan Y et al (2017) Imaging features from pre-treatment CT scans are associated with clinical outcomes in non-small cell lung cancer patients treated with stereotactic body radiotherapy. Med Phys 44(8):4341–4349

Oxnard GR, Binder A, Jänne PA (2013) New targetable oncogenes in non–small-cell lung cancer. J Clin Oncol 31:1097–1104

Raghunath S, Maldonado F, Rajagopalan S et al (2014) Noninvasive risk stratification of lung adenocarcinoma using quantitative computed tomography. J Thorac Oncol 9:1698–1703

Saad M, Choi TS (2017) Deciphering unclassified tumors of non-small-cell lung cancer through radiomics. Comput Biol Med 91:222–230

Saad M, Choi TS (2018) Computer-assisted subtyping and prognosis for non-small cell lung cancer patients with unresectable tumor. Comput Med Imaging Graph 67:1–8

Saad M, Lee IH, Choi T-S (2019) Automated delineation of non-small cell lung cancer: a step toward quantitative reasoning in medical decision science. Int J Imaging Syst Technol. https://doi.org/10.1002/ima.22336

Sacconi B, Anzidei M, Leonardi A et al (2017) Analysis of CT features and quantitative texture analysis in patients with lung adenocarcinoma: a correlation with EGFR mutations and survival rates. Clin Radiol 72:443–450

Siegel RL, Miller KD, Jemal A (2017) Cancer statistics 2017. CA: Cancer J Clin 67:7–30

Song J, Liu Z, Zhong W et al (2016) Non-small cell lung cancer: quantitative phenotypic analysis of CT images as a potential marker of prognosis. Sci Rep 6:38282

Tarsitano A, Ricotta F, Cercenelli L, Bortolani B et al (2019) Pretreatment tumor volume and tumor sphericity as prognostic factors in patients with oral cavity squamous cell carcinoma. J Cranio-Maxillofacial Surg 47(3):510–515

Thomas GB Jr, Finney RL (1979) Calculus and analytic geometry. Addison Wesley Publishing Company, Boston, p 434

Wang XZ, Cheng Y, Wang KL et al (2016) Peperomin E reactivates silenced tumor suppressor genes in lung cancer cells by inhibition of DNA methyltransferase. Cancer Sci 107:1506–1519

Zhao B, James LP, Moskowitz CS et al (2009) Evaluating variability in tumor measurements from same-day repeat CT scans of patients with non-small cell lung cancer. Radiology 252:263–272